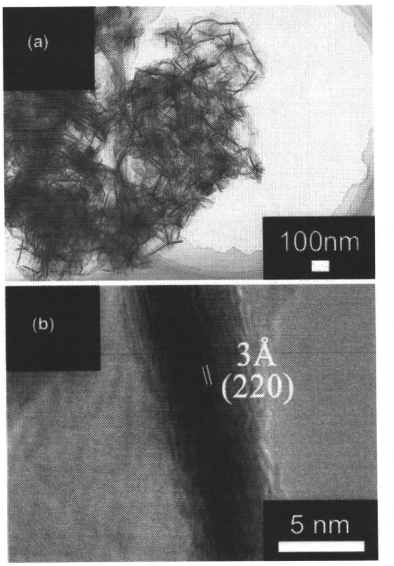

Fig. 6 TEM images of the synthesized Fe_3O_4. **a** TEM image and **b** HRTEM image

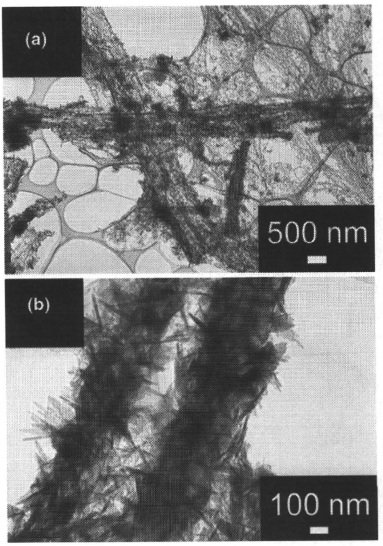

Fig. 7 TEM images of the synthesized cFF–Fe_3O_4 conjugate. **a** Low magnification and **b** high magnification

TEM images in this study implied that the self-assembly of cFF to form a rod-like morphology was not affected by the simultaneous synthesis of needle-shaped Fe_3O_4 NPs.

To evaluate magnetic property of the products and the mass of Fe_3O_4 in the cFF–Fe_3O_4 conjugate, superconducting quantum interference device (SQUID) magnetometry of the cFF–Fe_3O_4 conjugate was performed. The magnetic properties of the cFF–Fe_3O_4 conjugate and the synthesized needle-shaped Fe_3O_4 NPs were measured by using SQUID at 300 K (Fig. 8). The saturation moments of the cFF–Fe_3O_4 conjugate and the needle-shaped Fe_3O_4 NPs were 2.18 and 63.45 emu/g, respectively (Fig. 8a). However, the needle-shaped Fe_3O_4 NPs included the 4.3 wt% of organic molecules (see Fig. S3a in Supporting Information). To estimate the contribution of the Fe_3O_4 particles in the Fe_3O_4 nanoneedle, $M_{Fe_3O_4}$, was calculated using the equation described below

$$M_{Fe_3O_4} = \frac{M_{observed}}{(W_{sample} - W_{org})}$$

where $M_{observed}$, W_{sample}, and W_{org}, are the observed saturation magnetization value of the Fe_3O_4 nanoneedle with SQUID, the weight of the measured Fe_3O_4 nanoneedle, and the weight of the organic molecules included in the needle-shaped Fe_3O_4 NPs as estimated by TG measurement data respectively. The saturation magnetic moment of pure Fe_3O_4 included in the Fe_3O_4 nanoneedle was 66.58 emu/g. The amount of Fe_3O_4 present in the cFF–Fe_3O_4, $W_{Fe_3O_4}$, was calculated using the equation described below

$$W_{Fe_3O_4} = \frac{M_{cFF-Fe_3O_4}}{M_{Fe_3O_4}}$$

where $W_{Fe_3O_4}$, $M_{cFF-Fe_3O_4}$, and $M_{Fe_3O_4}$, are the amount of Fe_3O_4 present in the cFF–Fe_3O_4, the observed magnetization value of Fe_3O_4, and the calculated magnetization value of the needle-shaped Fe_3O_4 NPs,

respectively. The amount of Fe_3O_4 present in the cFF–Fe_3O_4 was 3.3 wt%.

Both the TEM and SQUID results indicate that the Fe_3O_4 nanoneedle were present on the surface of the cFF nanorods. In addition, the cFF–Fe_3O_4 conjugate and Fe_3O_4 nanoneedle showed almost the same coercivity about 100 Oe at 300 K (Fig. 8b).

To obtain information regarding the organic molecular structure, the Fourier transform infrared (FT-IR) spectra were measured (Fig. 9). In the case of the cFF–Fe_3O_4 conjugate (Fig. 9b), all peaks were identical to those of cFF synthesized without Fe_3O_4 (Fig. 9a). In addition, the FT-IR patterns were well matched with that of cFF synthesized using a previously described organic synthesis method (Brown et al. 1965). This result suggests that cFF constitutes the only organic component in the cFF–Fe_3O_4 conjugate.

The FT-IR spectra of L-Phe and the synthesized needle-shaped Fe_3O_4 NPs are shown in Fig. 9c and d, respectively. All the peaks in the L-Phe spectrum were assigned as per the data provided by Mahalakshmi et al. (2006) (see Table S1 in Supporting Information). In the FT-IR spectrum of the synthesized Fe_3O_4 (Fig. 9d), a broad band at 1584 cm^{-1} is visible; this band can be assigned as $n_{as}(COO^-)$ bound to the transition metal (Nakamoto 1970). Furthermore, the peaks at 1493, 1453, 1410, 1308, 1152, 1018, and 849 cm^{-1} can be assigned as $\beta_s(NH_3^+)$, $\nu(C–C)_{ring}$ + $b_s(CH_2)$, $n_s(COO^-)$, $\gamma_{as}(CH_2)$, $\delta(C–H)_{ring}$, $\Delta(C–H)_{ring}$, and $\gamma(C–H)_{ring}$, respectively. Thus, the obtained results

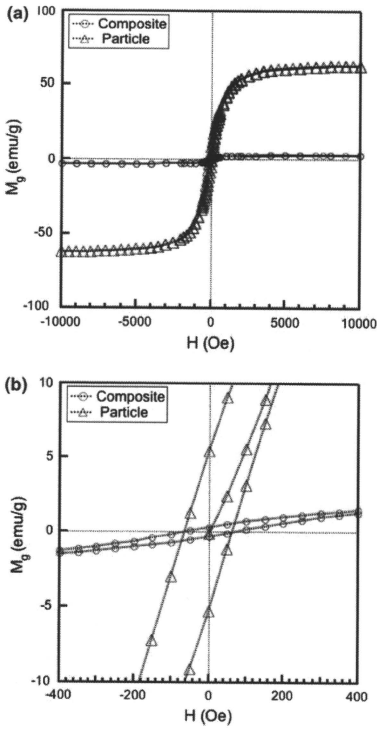

Fig. 8 Magnetic properties of the synthesized materials at 300 K (*open circle*: cFF–Fe_3O_4 conjugate, *open triangle*: synthesized Fe_3O_4 with 100 mM L-Phe)

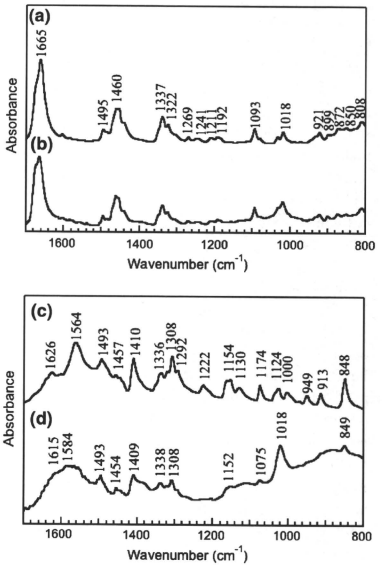

Fig. 9 FT-IR spectrum of (*a*) synthesized crystals with 710 mM of L-Phe, (*b*) synthesized crystal with 710 mM L-Phe and 50 mM $FeSO_4$, (*c*) pure L-Phe, and (*d*) synthesized crystal with 100 mM L-Phe and 50 mm $FeSO_4$

suggest the conjugation of L-Phe on Fe_3O_4 during the hydrothermal reaction.

Carny et al. reported that peptide-coated gold (Au) NPs could bind with peptide-based nanofibers in an aligned manner (Carny et al. 2006). The peptide that was conjugated on the Au NPs exhibited affinity toward the peptide nanofiber; as a result, the conjugated Au NPs could interact with the peptide nanofiber. This peptide–peptide interaction may constitute one of the main driving forces in the arrangement of Au NPs on the peptide nanofiber. In our study, the synthesized Fe_3O_4 nanoneedle is covered with L-Phe. The conjugated L-Phe and synthesized cFF have an aromatic ring at their side chain. It is possible that these aromatic rings undergo p–p interactions with each other. Thus, we consider that the π–π interaction between cFF and L-Phe conjugated on the Fe_3O_4 nanoneedle serves as one of the driving forces in the adherence of the Fe_3O_4 nanoneedles to the cFF nanorod.

A cFF–Fe_3O_4 conjugate was synthesized in situ by a one-pot hydrothermal reaction. The morphology of Fe_3O_4 changed from spherical and cubic shapes to a needle-like shape on account of the capping of L-Phe on the Fe_3O_4 surface. Fe_3O_4 nanoneedles were assembled on cFF rod-like crystals by hydrothermal synthesis under a high cFF concentration. This method may be applied to the production of NP arrays of various metal oxides from metal ions and amino acids and to the synthesis of rod-like cFF–metal oxide NP hybrids.

Conclusion

A cFF–Fe_3O_4 conjugate was synthesized in situ by a one-pot hydrothermal reaction. The morphology of Fe_3O_4 changed from spherical and cubic shapes to a needle-like shape on account of the capping of L-Phe on the Fe_3O_4 surface. Fe_3O_4 nanoneedles were assembled on cFF rod-like crystals by hydrothermal synthesis under a high cFF concentration. This method may be applied to the production of NP arrays of various metal oxides from metal ions and amino acids, L-Phe, and to the synthesis of rod-like cFF–metal oxide NP hybrids.

Acknowledgment This work was partly supported in part by a Grant-in-Aid for the COE project Giant Molecules and Complex Systems, 2002.

References

Alivisatos P (2004) The use of nanocrystals in biological detection. Nat Biotechnol 22:47–52. doi:10.1038/nbt927

Banerjee IA, Yu L, Matsui H (2005) Room-temperature Wurtzite ZnS nanocrystal growth on Zn finger-like peptide nanotubes by controlling their unfolding peptide structures. J Am Chem Soc 127:16002–16003. doi:10.1021/ja054907e

Braun E, Eichen Y, Sivan U, Ben-Yoseph G (1998) DNA-templated assembly and electrode attachment of a conducting silver wire. Nature 391:775–778. doi:10.1038/35826

Brown R, Kelley C, Wiberley SE (1965) The production of 3-benzylidene-6-isobutylidene-2,5-dioxopiperazine, 3,6-dibenzylidene-2,5-dioxopiperazine, 3-benzyl-6-benzylidene-2,5-dioxopiperazine, and 3,6-dibenzyl-2,5-dioxopiperazine by a variant of *Streptomyces noursei*. J Org Chem 30:277–280. doi:10.1021/jo01012a066

Byrappa K, Adschiri T (2007) Hydrothermal technology for nanotechnology. Prog Cryst Growth Chem 53:117–166. doi:10.1016/j.pcrysgrow.2007.04.001

Carny O, Shelev DE, Gazit E (2006) Fabrication of coaxial metal nanocables using a self-assembled peptide nanotube scaffold. Nano Lett 6:1594–1597. doi:10.1021/nl0604681

Claridge SA, Castleman AW, Khanna SN, Murray CB, Sen A, Weiss PS (2009) Cluster-assembled materials. ACS Nano 3:244–255. doi:10.1021/nn800820e

Collier CP, Vossmeyer T, Hearth JR (1998) Nanocrystal superlattices. Annu Rev Phys Chem 49:371–404. doi:10.1146/annurev.physchem.49.1.371

Cornell RM, Schwertmann U (2003) The iron oxides, 2nd edn. Wiley–VCH Verlag GmbH & Co

Fan HM, Yi JB, Yang Y, Kho KW, Tan HR, Shen ZX, Ding J, Sun XW, Olivo MC, Feng YP (2009) Single-crystalline MFe_2O_4 nanotubes/nanorings synthesized by thermal transformation process for biological applications. ACS Nano 3:2798–2808. doi:10.1021/nn9006797

Feng J, Miedaner A, Ahrenkiel P, Himmel ME, Curtis C, Ginley D (2005) Self-assembly of photoactive TiO_2-cyclodextrin wires. J Am Chem Soc 127:14968–14969. doi:10.1021/ja054448h

Fu X, Wang Y, Huang L, Sha Y, Gui L, Lai L, Tang Y (2003) Assemblies of metal nanoparticles and self-assembled peptide fibrils—formation of double helical and single-chain arrays of metal nanoparticles. Adv Mater 15:902–906. doi:10.1002/adma.200304624

Gasser U (2009) Crystallization in three- and two-dimensional colloidal suspensions. J Phys Condens Mater 21:203101-1-14. doi:10.1088/0953-8984/21/20/200301

Gdaniec M, Liberek B (1986) Structure of cyclo(-L-phenylalanyl-L-phenylalanyl-). Acta Crystallogr Sect C: Cryst Struct Commun 42:1343–1345. doi:10.1107/S0108270186092338

Hatakeyama Y, Minami M, Ohara S, Umetsu M, Takami S, Adschiri T (2004) Control of designed high-order DNA conformation as a template for nano particle assembly. Kobunshironbunsyu 61:617–622

Huang J, Kunitake T (2003) Nano-precision replication of natural cellulosic substances by metal oxides. J Am Chem Soc 125:11834–11835. doi:10.1021/ja037419k

Hultgren A, Tanase M, Chen CS, Meyer GJ, Reiche DH (2003) Cell manipulation using magnetic nanowires. J Appl Phys 93:7554–7556. doi:10.1063/1.1556204

Mahalakshmi R, Jesuraja SX, Jerome DS (2006) Growth and characterization of L-phenylalanine. Cryst Res Technol 41:780–783. doi:10.1002/crat.200510668

Nakamoto K (1970) Infrared spectra of inorganic and coordination compounds, 2nd edn. Willy–Interscience, pp 232–239

Nie Z, Petukhova A, Kumacheva E (2010) Properties and emerging applications of self-assembled structures made from inorganic nanoparticles. Nat Nanotechnol 5:15–25. doi:10.1038/nnano.2009.453

Ostrov N, Gazit E (2010) Genetic engineering of biomolecular scaffolds for the fabrication of organic and metallic nanowire. Angew Chem Int Ed 49:3018–3021. doi:10.1002/anie.200906831

Patolsky F, Weizmann Y, Willner I (2004) Actin-based metallic nanowires as bio-nanotransporters. Nat Mater 3:692–695. doi:10.1038/nmat1205

Pileni MP (2001) Nanocrystal self-assemblies: fabrication and collective properties. J Phys Chem B 105:3358–3371. doi:10.1021/jp0039520

Platt M, Muthukrishnan G, Hancock WO, Williams ME (2005) Millimeter scale alignment of magnetic nanoparticle functionalized microtubles in magnetic fields. J Am Chem Soc 127:15686–15687. doi:10.1021/ja055815s

Sarikaya M, Tamerler C, Jen AK-Y, Schulten K, Baneyx F (2003) Molecular biomimetics: nanotechnology through biology. Nat Mater 2:577–585. doi:10.1038/nmat964

Scheibel T, Parthasarathy R, Sawicki G, Lin XM, Jaeger H, Lindquist SL (2003) Conducting nanowires built by controlled self-assembly of amyloid fibers and selective metal deposition. Proc Natl Acad Sci USA 100:4527–4532. doi:10.1073_pnas.0431081100

Sone ED, Stupp SI (2004) Semiconductor-encapsulated peptide-amphiphile nanofibers. J Am Chem Soc 126:12756–12757. doi:10.1021/ja0499344

Sugimoto T, Muramatsu A, Sakata K, Shindo D (1993) Characterization of hematite particles of different shapes. J Colloid Interf Sci 158:420–428. doi:10.1006/jcis.1993.1274

Tan ST, Wendorff JH, Pietzonka C, Jia ZH, Wang GQ (2006) Biocompatible and biodegradable polymer nanofibers displaying superparamagnetic properties. Chem Phys Chem 6:1461–1465. doi:10.1002/cphc.200500167

Tang T, Kotov NA (2005) One-dimensional assemblies of nanoparticles: preparation, properties, and promise. Adv Mater 17:951–962. doi:10.1002/adma.200401593

Togashi T, Umetsu M, Tsuchizaki H, Ohara S, Naka T, Adschiri T (2006) Simultaneous synthesis and self-assembly of cyclic diphenylalanine at hydrothermal condition. Chem Lett 35:636–637. doi:10.1246/cl2006.636

Wang Y, Li YF, Huang CZ (2009) A one-pot green method for one-dimensional assembly of gold nanoparticles with a novel chitosan-ninhydrin bioconjugate at physiological temperature. J Phys Chem C 113:4315–4320. doi:10.1021/jp809708q

Xia Y, Xiong Y, Lim B, Skrabalak SE (2009) Shape-controlled synthesis of metal nanocrystals: simple chemistry meets complex physics? Angew Chem Int Ed 48:60–103. doi:10.1002/anie.200802248

Yoshimura M, Byrappa K (2008) Hydrothermal processing of materials: past, present and future. J Mater Sci 43:2085–2103. doi:10.1007/s10853-007-1853-x

Enhancement of Cellulolytic Enzyme Activity by Clustering Cellulose Binding Domains on Nanoscaffolds

Do-Myoung Kim, Mitsuo Umetsu, Kyo Takai, Takashi Matsuyama, Nobuhiro Ishida, Haruo Takahashi, Ryutaro Asano, and Izumi Kumagai*

Cellulose, one of the most abundant carbon resources, is degraded by cellulolytic enzymes called cellulases. Cellulases are generally modular proteins with independent catalytic and cellulose-binding domain (CBD) modules and, in some bacteria, catalytic modules are noncovalently assembled on a scaffold protein with CBD to form a giant protein complex called a cellulosome, which efficiently degrades water-insoluble hard materials. In this study, a catalytic module and CBD are independently prepared by recombinant means, and are heterogeneously clustered on streptavidin and on inorganic nanoparticles for the construction of artificial cellulosomes. Heteroclustering of the catalytic module with CBD results in significant improvements in the enzyme's degradation activity for water-insoluble substrates. In particular, the increase of CBD valency in the cluster structure critically enhances the catalytic activity by improving the affinity for substrates, and clustering with multiple CBDs on CdSe nanoparticles generates a 7.2-fold increase in the production of reducing sugars relative to that of the native free enzyme. The multivalent design of substrate-binding domain on clustered cellulases is important for the construction of the artificial cellulosome, and the nanoparticles are an effective scaffold for increasing the valence of CBD in clustered cellulases. A new design is proposed for artificial cellulosomes with multiple CBDs on noncellulosome-derived scaffold structures.

1. Introduction

Recent advances in bioconjugate technology have supplied various concepts for covalent and noncovalent linkages between proteins, which allow us to artificially assemble functional proteins. For example, the coupling between a specific pair of fluorescent proteins can transfer fluorescence energy so as to detect intermolecular interactions,[1] and the assembly of antibody fragments via protein–protein interactions increases the valence of antigen-binding sites to improve therapeutic effects in treating cancer tumors.[2] Furthermore, nanoscale structural designs obtained by molecular assembly and by downsizing of inorganic materials are enabling the fabrication of higher-order functional devices by utilizing the nanomaterials as scaffolds for assembling functional proteins. Protein cages, such as ferritin and viruses, have been widely used as nanoscale building blocks for higher-order nanostructures.[3–5] Additionally, adjacent attachment of cofactor–enzyme pairs on self-assembled DNA scaffolds induces designed cascade chemical reactions,[6] and the clustering of antibodies on nanoparticles generates high avidity that critically improves the binding of antibodies for antigen-displayed substrates and cell surfaces.[7–9]

D.-M. Kim, Dr. M. Umetsu, K. Takai, Dr. R. Asano, Prof. I. Kumagai
Department of Biomolecular Engineering
Graduate School of Engineering
Tohoku University
Aoba 6-6-11, Aramaki, Aoba-ku, Sendai, 980–8579, Japan
E-mail: mitsuo@kuma.che.tohoku.ac.jp
Dr. M. Umetsu
Center for Interdisciplinary Research
Tohoku University
Aoba 6–3, Aramaki, Aoba-ku, Sendai, 980–8578, Japan
Dr. T. Matsuyama, Dr. N. Ishida, Dr. H. Takahashi
Toyota Central R&D Lab
Yokomichi 41–1, Oaza Nagakute,
Nagakute-cho, Aichi-gun, 480–1192, Japan

DOI: 10.1002/smll.201002114

NANO MICRO small

Clustering of functional proteins is also utilized for improving the reaction efficiencies of enzymes in some bacteria. Cellulose, which is a linear polysaccharide polymer of glucosyl units connected by β-1,4-linkages, is an abundant carbon resource on earth and an energy source for cellulolytic bacteria and fungi. Cellulose is a water-insoluble hard material, but bacteria and fungi degrade the material to low-molecular-weight sugars by means of cellulolytic enzymes called cellulases. Cellulases are generally modular proteins with independent catalytic and cellulose-binding domain (CBD) modules, and in some bacteria, catalytic modules with different functions are clustered on a giant scaffold protein with CBD via cohesin–dockerin interactions to improve the degradation efficiency of the catalytic module.[10,11] The dockerin domain in catalytic modules interacts noncovalently with one of the cohesin domains tandemly arranged in the giant scaffold protein to form a complicated protein complex called a cellulosome. The clustered catalytic modules are adsorbed on cellulose via CBD in the scaffold protein and synergistically degrade biomass materials by means of coupled hydrolysis reactions.[12,13]

High performance of cellulosomes with regard to their efficiency of degradation is attractive for the production of alternative fuels from renewable biomass resources with low energetic and environmental loads. However, extracting substantial amounts of cellulosomes from native bacteria is too difficult to utilize native cellulosomes for the production of alternative fuels. Several studies have reported the preparation of small cellulosomes from recombinant proteins expressed in *Escherichia (E.) coli*,[12,14–16] but the recombinant preparation of intact cellulosomes with the same length and activity as those of the native form remains challenging. Therefore, a new means of fabricating highly clustered enzyme complexes is needed.

In this study, a new design for artificial cellulosomes is proposed from recombinant enzyme modules on noncellulosome-derived scaffold structures. Cellulases are traditionally classified into endoglucanases, cellobiohydrolases, and β-glucosidases: endoglucanases prefer to randomly hydrolyze amorphous celluloses to cellooligosaccharides, cellobiohydrolases can degrade crystalline cellulose from the chain ends to cellobiose, and released short cellobioses are finally degraded to glucoses by β-glucosidases.[17–19] Here, endoglucanase A (EglA) were clustered from *Aspergillus niger*[20] as a catalytic module and the second N-terminal CBD in endoglucanse C from *Cellulomonas fimi*[21,22] as a CBD on streptavidin and on streptavidin-immobilized inorganic nanoparticles (**Scheme 1**). EglA has only a catalytic domain, and the CBD used selectively binds to amorphous celluloses.

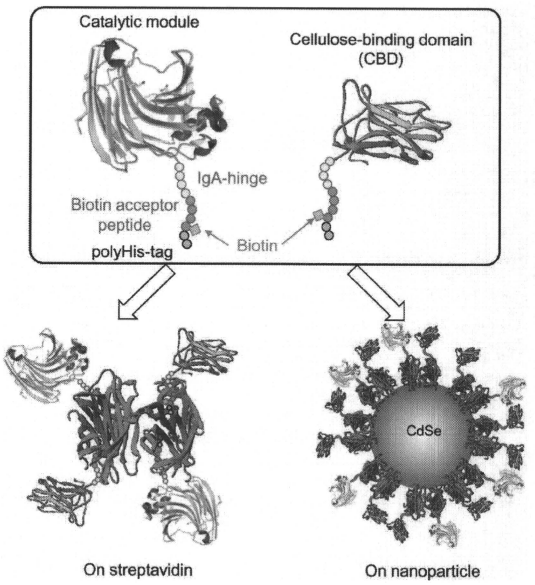

Scheme 1. Schematic illustration of the clustering of catalytic and cellulose-binding domain (CBD) modules on streptavidin and on nanoparticles. The polyHis-tag is the peptide of polyhistidine (HHHHHH), which is utilized for protein purification by means of a metal–chelate chromatography column.

Homoclustering of catalytic modules only slightly improves the degradation of water-insoluble celluloses, but the increment of CBD in clustered complexes critically enhances their catalytic activity, with heteroclustering on nanoparticles resulting in a 9.6-fold increase relative to the native EglA's activity. Here, the ability of in-vitro assembly to improve the reaction efficiencies of enzymes and the potential of nanoparticles to serve as a giant scaffold structure for the construction of artificial cellulosomes is demonstrated.

2. Results

2.1. Heteroclustering of EglA and CBD on Streptavidin

EglA and CBD modules with a biotin acceptor peptide were independently prepared in *E. coli* within biotin ligase by recombinant means (see Experimental Section), so that the recombinant EglA and CBD modules had a biotin molecule only in the peptide tag (see Scheme 1). In all the experiments, the recombinant EglA and CBD was used, each with a biotinylated tag at their C-terminus, as biotinylated proteins. These biotinylated EglA and CBD were mixed with streptavidin at different molecular ratios (EglA:CBD:streptavidin = 3:1:1,

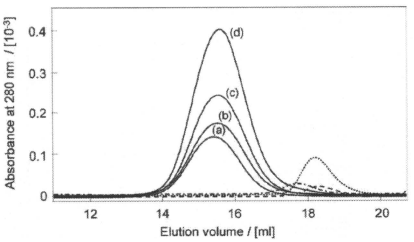

Figure 1. Size-exclusion chromatography of clustered EglA–CBD complexes on streptavidin. Dotted line: 4 μM EglA; dashed line: 4 μM CBD; dotted and dashed line: 4 μM streptavidin; a) 4 μM EglA with 1 μM streptavidin; b) mixture of 4 μM EglA and 1.3 μM CBD with 1.3 μM streptavidin; c) mixture of 4 μM EglA and 4 μM CBD with 2 μM streptavidin; d) mixture of 4 μM EglA and 12 μM CBD with 4 μM streptavidin. Each 500 μL sample solution was applied to the column, and the absorbance of the eluent was monitored at 280 nm.

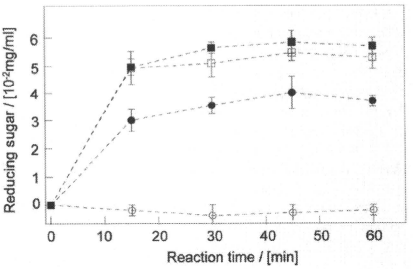

Figure 2. Amounts of reducing sugars produced from 1 mg mL^{-1} CMC in a 50 mM sodium acetate solution (pH 5.0, 200 mM NaCl) at 40 °C for 60 min in the presence of no protein (open circles), 0.4 μM EglA (closed circles), 0.4 μM EglA and 1.2 μM CBD (open squares), EglA–CBD clusters containing 0.4 μM EglA, 1.2 μM CBD, and 0.4 μM streptavidin (closed squares). All experiments were conducted three times and average values were plotted with error bars of standard variation.

2:2:1, 1:3:1) to yield several complexes in which EglA and CBD were clustered on streptavidin at different ratios. **Figure 1** shows size-exclusion chromatography results for the clustered complexes. In the absence of streptavidin, biotinylated EglA and CBD (31 kDa and 21 kDa, respectively) were eluted at fractions of 18.2 mL and 18.3 mL, respectively, which correspond to each monomeric form. In contrast, in the presence of streptavidin, no monomeric biotinylated EglA and CBD were observed (Figure 1, dotted and dashed lines, respectively); instead, a fraction eluted at ≈15.4–15.6 mL, which corresponds to the proteins with ≈19–16 kDa, was observed (Figure 1, lines a–d). This result shows that all the biotinylated EglA and CBD were clustered on streptavidin. As the amount of added CBD increased, the eluted fractions containing clustered complexes were slightly shifted toward lower molecular weights, implying that the ratio of CBD in the clustered complexes increased.

2.2. Degradation Activity of EglA–CBD Cluster on Streptavidin for Water-Soluble and -Insoluble Cellulose Substrates

To analyze the enzyme activity of the EglA–CBD cluster on streptavidin for cellulose substrates, the degradation activity for carboxymethyl cellulose (CMC) and phosphoric-acid–swollen cellulose (PSC) was measured by means of a tetrazolium blue chloride (TZ) assay. The concentration of EglA in the reaction solution was adjusted to 0.4 μM to analyze the activity change of EglA in the clusters. CMC substrates are soluble celluloses in water, but PSC are water-insoluble amorphous celluloses. **Figure 2** shows the amount of reducing sugars produced from CMC. Biotinylated EglA without CBD and streptavidin degraded CMC to produce ≈0.037 mg mL^{-1} reducing sugars in 60 min (closed circles). The degradation activity of EglA for CMC was slightly improved in the presence of CBD (open squares), and the clustering of EglA together with CBD on streptavidin also caused a slight improvement in enzyme activity (closed squares). This result implies that the clustering event slightly influences EglA's degradation activity for water-soluble CMC.

For water-insoluble PSC, the activity of EglA was much weaker than that observed for CMC (**Figure 3**): free EglA alone degraded PSC into less than 0.01 mg mL^{-1} reducing sugars in 60 min (open circles), indicating that EglA hardly accessed the insoluble cellulose material. The addition of CBD without streptavidin and the clustering of EglA on streptavidin without CBD resulted in only a slight improvement of EglA activity (closed circles and open squares, respectively), but the clustering of EglA together with CBD

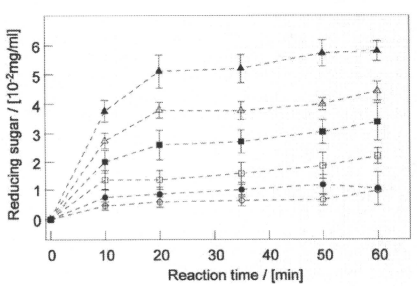

Figure 3. Amounts of reducing sugars produced from 1 mg mL^{-1} PSC at 40 °C for 60 min in the presence of 0.4 μM EglA (open circles), 0.4 μM EglA and 1.2 μM CBD (closed circles), and EglA–CBD clusters containing 0.4 μM EglA, 0 μM CBD, and 0.1 μM streptavidin (open squares), 0.4 μM EglA, 0.13 μM CBD, and 0.13 μM streptavidin (closed squares), 0.4 μM EglA, 0.4 μM CBD, and 0.2 μM streptavidin (open triangles), and 0.4 μM EglA, 1.2 μM CBD, and 0.4 μM streptavidin (closed triangles). All experiments were conducted three times and average values were plotted with error bars of standard variation.

NANO MICRO small

on streptavidin showed a distinct effect: as the amount of CBD increased, the degradation activity of EglA for PSC was drastically enhanced to produce ≈0.058 mg mL^{-1} reducing sugars (closed triangles). CMC is soluble in water, but water-insoluble PSC forms some molecular aggregate structures. Therefore, these results indicate that the multivalency of CBD is effective for the enhancement of enzyme activity for substrates with insoluble aggregated structures in water.

2.3. Clustering of EglA and CBD on Streptavidin-Conjugated CdSe Nanoparticles

To increase the valence of CBD in EglA–CBD clusters, streptavidin-conjugated, 20 nm cadmium selenide (CdSe) nanoparticles were used to promote high-order clustering of biotinylated EglA and CBD. Each CdSe nanoparticle was conjugated with 5–10 streptavidins, so that ≈30 biotin molecules could be bound on the surface of CdSe nanoparticles. **Figure 4** shows the binding of streptavidin-conjugated CdSe nanoparticles onto PSC substrates after biotinylated EglA and CBD were mixed. Little fluorescence from CdSe nanoparticles was detected on precipitated PSC in the absence of CBD (Figure 4A), whereas CdSe nanoparticles clustered with biotinylated CBD were immobilized on PSC (Figure 4B). These results confirm the immobilization of CBD on the nanoparticles and the subsequent binding of the nanoparticles to the PSC surface.

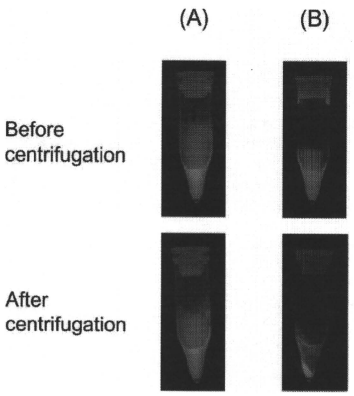

Figure 4. Fluorescence analysis of the adsorption of streptavidin-conjugated CdSe nanoparticles onto PSC substrates. Mixtures of 53 nM CdSe nanoparticles in a 50 mM sodium acetate solution (pH 5.0, 200 mM NaCl) containing 1 mg mL^{-1} PSC were centrifuged. A) Untreated CdSe nanoparticles; B) CdSe nanoparticles containing 0.4 μM EglA and 1.2 μM CBD.

2.4. Degradation Activity of Nanoparticles Conjugated with EglA and CBD for PSC

Figure 5 shows the degradation activity of CdSe nanoparticles conjugated with EglA and CBD for PSC substrates. The changes in degradation activity for PSC observed after clustering of EglA and CBD on the nanoparticles were similar to those observed for clustered EglA on streptavidin: nanoparticles conjugated with only EglA showed a slight promotion of PSC degradation (open squares in Figure 5A), but nanoparticles conjugated with both EglA and CBD exhibited drastically enhanced activity as the amount of added CBD increased (closed squares, and open and closed triangles in Figure 5A). The nanoparticles conjugated with EglA and CBD at a ratio of 1:3 produced ≈0.065 mg mL^{-1} reducing sugars for 60 min, which were comparable to those

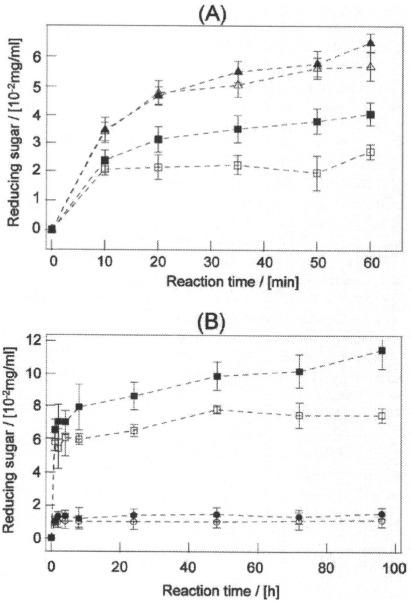

Figure 5. Amounts of reducing sugars produced from 1 mg mL^{-1} PSC at 40 °C. A) Degradation reaction for 60 min in the presence of 13.3 nM CdSe nanoparticles with 0.4 μM EglA (open squares), 17.8 nM CdSe with 0.4 μM EglA and 0.13 μM CBD (closed squares), 26.7 nM CdSe with 0.4 μM EglA and 0.4 μM CBD (opend triangles), 53.3 nM CdSe with 0.4 μM EglA and 1.2 μM CBD (closed triangles). B) Degradation reaction for 96 h in the presence of 0.4 μM EglA (open circles), 0.4 μM EglA and 1.2 μM CBD (closed circles), EglA–CBD clusters containing 0.4 μM EglA, 1.2 μM CBD, and 0.4 μM streptavidin (open squares), and 53.3 nM CdSe nanoparticles with 0.4 μM EglA and 1.2 μM CBD (closed squares). All experiments were conducted three times and average values were plotted with error bars of standard variation.

produced by the EglA–CBD clusters on streptavidin at a ratio of 1 EglA:3 CBD:1 streptavidin (closed triangles in Figure 3).

Further, the amount of reducing sugars produced from PSC over 96 h was measured (Figure 5B). It was determined that the amount of reducing sugars produced after 96 h by the nanoparticles conjugated with EglA and CBD at a ratio of 1:3 was about 1.6 times as much as the amount of reducing sugars produced by EglA–CBD clustered on streptavidin. After more than 1 h, the clustering of EglA and CBD on nanoparticles produced more reducing sugars than the clustering on streptavidin.

2.5. Quantitative Analysis for Degradation Activity of EglA–CBD Clusters

To quantitatively analyze the enhancement of degradation activity for PSC, the degradation rate of EglA–CBD clusters was measured for 60 s at various PSC concentrations to estimate the Michaelis–Menten constant (K_m) and turnover number (k_{cat}) from Lineweaver–Burk plots (**Figure 6**). The clustering of EglA and CBD at a ratio of 1:3 showed a drastic increase in the initial degradation rates (Figure 6A), and the initial rates calculated from the reactions after only 20 s show good correlation with the Lineweaver–Burk plot (Figure 6B).

Table 1 lists the K_m and k_{cat} values of EglA–CBD clusters estimated from the Lineweaver–Burk plot. The K_m and k_{cat} values of both the EglA–CBD clusters on streptavidin and on nanoparticles demonstrate that the clustering of EglA and CBD contributes to the increase of both the affinity of EglA for substrates and the reaction rate of EglA. However, the factor predominantly contributing to activity enhancement is dependent on the clustering format: the enhancement of degradation activity by clustering on streptavidin is predominantly attributed to the increase of reaction rates, but the clustering on nanoparticles significantly increased the affinity for substrates. This difference implied that the mechanism of activity enhancement by clustering is different between the EglA–CBD clusters on streptavidin and on nanoparticles.

In addition, the equilibrium dissociation constant (K_d) of EglA-CBD clusters for PSC was measured (Table 1) and significant decreases of K_d values by clustering with CBD were confirmed. These results imply that the enhancement of the affinity for PSC is a contributory factor to the increase of K_m values.

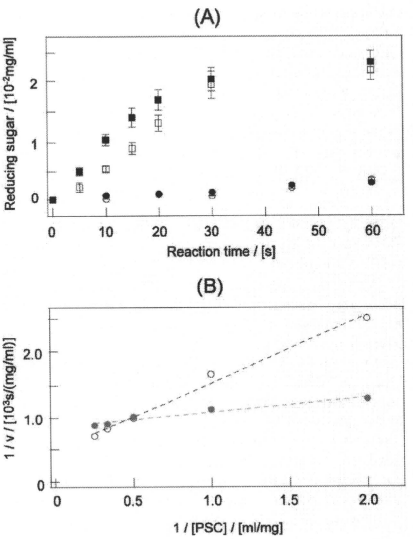

Figure 6. A) Amounts of reducing sugars produced from 1 mg mL^{-1} PSC at 40 °C for 60 s in the presence of 0.4 μM EglA (open circles), 0.4 μM EglA and 1.2 μM CBD (closed circles), EglA–CBD clusters containing 0.4 μM EglA, 1.2 μM CBD, and 0.4 μM streptavidin (open squares), and 53.3 nM CdSe nanoparticles with 0.4 μM EglA and 1.2 μM CBD (closed squares). All experiments were conducted three times and average values were plotted with error bars of standard variation. B) Lineweaver–Burk plots for EglA–CBD clusters on streptavidin (black open circles) and on nanoparticles (red closed squares).

2.6. Degradation Activity of Egla–CBD Clusters for Water-Insoluble Microcrystalline Cellulose Substrates

To analyze the enzyme activity of the EglA-CBD clusters for microcrystalline cellulose substrates, the degradation activity was measured for avicel substrates at an EglA concentration of 2 μM. The analysis for avicel substrates

Table 1. K_m, k_{cat}, and K_d values of EglA, CBD, and EglA–CDB clusters on streptavidin and on CdSe nanoparticles for the PSC substrate. The numbers in parentheses and in square brackets represent the ratio of clustered cellulases to free EglA activity, and the ratio of clustered cellulases to the activity of mixture of EglA and CBD without streptavidin and nanoparticles, respectively.

	K_m [mg mL^{-1}]	k_{cat} [10^{-3} mg mL^{-1} s^{-1} μM^{-1}]	Reducing sugar produced after 96 h [mg mL^{-1}]	K_d [nM]
EglA	5.94 ± 0.04 (1)	1.79 ± 0.04 (1)	0.012 ± 0.003 (1)	–
CBD	–	–	–	2.6 ± 0.3 × 10^3
1 EglA + 3 CBD	2.84 ± 0.03 (0.48) [1]	1.61 ± 0.02 (0.9) [1]	0.016 ± 0.003 (1.3) [1]	–
1 EglA + 3 CBD + 1 streptavidin	2.02 ± 0.11 (0.34) [0.71]	4.94 ± 0.32 (2.8) [3.1]	0.073 ± 0.004 (6.1) [4.6]	14 ± 2.6
7 EglA + 23 CBD + 1 CdSe	0.26 ± 0.06 (0.04) [0.091]	2.90 ± 0.24 (1.6) [1.8]	0.115 ± 0.011 (9.6) [7.2]	2 ± 0.7

NANO MICRO small

showed activity promotion of EglA upon clustering together with CBD on streptavidin (**Figure 7**A). Free EglA showed no degradation activity for avicel (open circles), and the addition of CBD without streptavidin had little influence on the activity (closed circles). Although the EglA-CBD clusters formed at ratios of 3 EglA:1 CBD and 2 EglA:2 CBD showed no activity for avicel (closed squares and open triangles, respectively), the clustering of EglA and CBD at a ratio of 1:3 on streptavidin promoted degradation of avicel to produce ≈0.017 mg mL^{-1}reducing sugars (closed triangles). The gradual enhancement of clustered EglA activity upon increasing the valence of CBD on streptavidin, which was observed for amorphous substrates (PSC), was also confirmed for crystalline substrates.

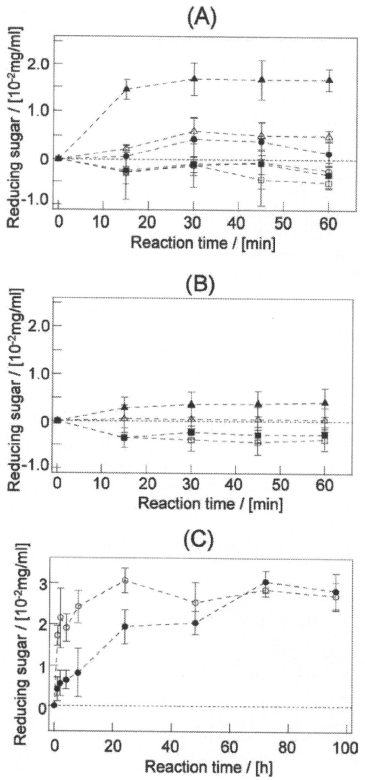

Figure 7. Amounts of reducing sugars produced from 1 mg mL^{-1} avicel in a 50 mM sodium acetate solution (pH 5.0, 200 mM NaCl) at 40 °C. A) Degradation reaction for 60 min in the presence of 2 μM EglA (open circles), 2 μM EglA and 6 μM CBD (closed circles), and EglA–CBD clusters containing 2 μM EglA, 0 μM CBD, and 0.5 μM streptavidin (open squares), 2 μM EglA, 0.67 μM CBD, and 0.67 μM streptavidin (closed squares), 2 μM EglA, 2 μM CBD, and 1 μM streptavidin (open triangles), and 2 μM EglA, 6 μM CBD, and 2 μM streptavidin (closed triangles). B) Degradation reaction for 60 min in the presence of 13.3 nM CdSe nanoparticles with 0.4 μM EglA (open squares), 17.8 nM CdSe with 0.4 μM EglA and 0.13 μM CBD (closed squares), 26.7 nM CdSe with 0.4 μM EglA and 0.4 μM CBD (open triangles), 53.3 nM CdSe with 0.4 μM EglA and 1.2 μM CBD (closed triangles). C) Degradation reaction for 96 h in the presence of EglA–CBD clusters containing 0.4 μM EglA, 1.2 μM CBD, and 0.4 μM streptavidin (open circles), and 53.3 nM CdSe nanoparticles with 0.4 μM EglA and 1.2 μM CBD (closed circles). All experiments were conducted three times and average values were plotted with error bars of standard variation.

The nanoparticles conjugated with EglA and CBD also showed similar activity enhancement to that observed for EglA–CBD clusters on streptavidin (Figure 7B): a conjugation of 1 EglA:3 CBD on the CdSe nanoparticles enabled the degradation of avicel substrates (closed triangles). Although the nanoparticles with EglA and CBD at a ratio of 1:3 produced less reducing sugars at the reaction time of 60 min than the clusters on streptavidin, the sugars were gradually produced as the reaction time increased; finally, at the reaction time of 96 h, the amount of produced sugars was comparable to that produced by EglA–CBD clusters on streptavidin (Figure 7C). This different behavior between the clustering on streptavidin and on nanoparticles suggests that the clustering format also influences the mechanism of degradation enhancement. Michaelis–Menten kinetic parameters were estimated, however, even after EglA was clustered with CBD, the activity for avicel was too weak to obtain reliable initial rates in replicate.

3. Discussion

3.1. Clustering of Cellulases via Biotin–Avidin Interactions

In this study, catalytic (EglA) and CBD modules were clustered on streptavidin and on CdSe nanoparticles via biotin–avidin interactions. Biotin–avidin linkages have been widely utilized because of their strong and specific noncovalent interactions, and a biotin acceptor peptide enables the structurally homogeneous tetramerization of recombinant proteins. Cloutier et al. fused the biotin acceptor peptide at the C-terminus of single-chain fragments of variable region (scFv) in antibodies via an IgA hinge linker, and the scFv fragments with only a biotin molecule on the acceptor peptide were tetramerized on streptavidin to show a 20–30-fold increase in equilibrium association constant compared with that of monomeric scFv.[23] This critical increase in binding affinity induced by the formation of multimeric antibodies is generally attributed to the slowing of the dissociation rate of the antigen, although the increase in binding valence can increase the chance of rapid and simultaneous contact to increase the association rate constant.[24]

Here, we applied the methodology of the scFv multimer formation to the clustering of cellulase modules, and further, we utilized nanoparticles as a scaffold backbone to generate a high multivalence of these modules. The fusion of a biotin acceptor peptide at the C-terminus of each recombinant module resulted in the assembly of EglA and CBD to form

highly active EglA–CBD clusters. Proteins can be chemically biotinylated via amino groups on the surface of the proteins. Therefore, we also tried chemical modification of biotin on EglA and CBD modules; however, the chemical modification heterogeneously conjugated biotin molecules on a module protein, and clustering with these proteins occurred with low efficiency, leading to multimerization of streptavidin via multibiotinylated EglA or CBD.

3.2. Effect of Heteroclustering on Degradation Activity

The clustering of EglA together with CBD on streptavidin resulted in little improvement of EglA's degradation activity for water-soluble substrates, but the activity of EglA–CBD clusters for water-insoluble substrates increased as the valence of CBD increased in the clustered complexes on streptavidin. Consequently, clustering on streptavidin and on CdSe nanoparticles resulted in significant improvement of degradation activity for PSC, and clustering on streptavidin and on the nanoparticles enabled the degradation of avicel (Figure 4,7).

Cellulases in cellulosomes show effective activity for cellulose material degradation, but individual cellulases separated from cellulosomes have low degradation activity.[14,15] Carrard et al. generated several recombinant CBD molecules with a cohesin domain: the cohesin-fused CBD spontaneously binds to dockerin-containing cellulases at a ratio of 1:1 to activate the enzymes for water-insoluble substrates.[25] In this study, we drastically increased the activation of the endoglucanase EglA by clustering it with CBD on streptavidin and on nanoparticles. Our design not only improved the degradation activity of EglA owing to its conjugation with CBD, but also showed the avidity effect caused by the multivalence of CBD on the degradation activity.

3.3. CBD Function

CBD plays a role in localizing catalytic modules in cellulolytic enzymes and cellulosomes on cellulose surfaces to substantially increase substrate concentration around catalytic domains. Various CBDs with different affinities and specificities for the surfaces of celluloses have been reported, but the binding functions of these CBDs can be divided into two main categories: reversibility and crystalline structure recognition.[26] A CBD reversibly or irreversibly binds onto a substrate surface, and the binding is specific for crystalline or amorphous substrates. The thermodynamic factors associated with the binding of CBD onto cellulose depend on the surface of substrates: enthalpy changes drive binding onto an amorphous surface,[27] such as in the cases of peptides and antibodies with affinities for inorganic material surfaces,[28–30] whereas CBD binding to crystalline structures is entropy-driven.[31]

In this study, we utilized the second N-terminal CBD of endoglucanse C from *Cellulomonas fimi*, which selectively binds to amorphous celluloses.[21,22] The fact that catalytic modules with multiple CBDs efficiently degraded water-insoluble substrates implies that the localization of enzymes on the substrate surface was a critical factor for degrading insoluble substrates: actually, the clustering of EglA with CBD both on streptavidin and nanoparticles increased the K_d values (Table 1). The clustered complexes with multiple CBD molecules further degraded the microcrystalline substrate avicel. The multivalence effect of CBD might have induced efficient localization of catalytic modules on the few amorphous areas of avicel.

The clustering of CBD both on streptavidin and on nanoparticles enhanced the degradation activity of EglA for water-insoluble substrates by improving the affinity for the substrate (K_m) and the degradation rate of EglA (k_{cat}), but the factor predominantly contributing to the activity enhancement was a dependence on the clustering format: the clustering on streptavidin increased the degradation rate of EglA, while the use of nanoparticles significantly enhanced the affinity for water-insoluble substrates. An increase of the number of CBD modules enhanced the binding to PSC substrates (see K_d values in Table 1) to increase the opportunity for active site of EglA to bind to degradable sites in PSC: actually, the nanoparticles with 7 EglA and 23 CBD showed much smaller K_m values than free EglA and EglA–CBD clusters on streptavidin. Whereas, the degradation reaction of EglA was also enhanced by the clustering with CBD, but small scale clustering on streptavidin was more effective than the use of nanoparticles as a scaffold. The localization of EglA on PSC could also improve the degradation reaction, but our results imply that the clustering structure is important for the degree of promotion.

In addition to the factors of reversibility and recognition, it should be noted that some CBDs bind to substrates to physically disrupt cellulosic fibers.[26] The addition of some family II CBDs in cellulose suspensions causes the release of noncovalently attached particles from cellulose fibers,[32,33] and the disruption of fiber agglomerates by CBD has been observed in scanning electron microscopy images.[34,35] Din et al. further reported that the simultaneous addition of a catalytic module and a family II CBD to cellulose suspension increased the hydrolytic activity of the catalytic modules.[33] In our results, the addition of unclustered CBD resulted increased the affinity of EglA for substrates (Table 1). If this improvement of affinity is due to the disruption function of the CBD used in this study, our results indicate that the disruption by CBD increases the opportunities of the adsorption of EglA.

Carrard et al. also reported that the binding properties of CBD influence the degradation activity of catalytic modules.[25] Our cluster design can easily be used to generate various cellulolytic enzymes with multiple types of CBDs. Heteroclustering experiments using different types of CBDs are in progress to examine possible synergy effects due to differing affinities and specificities among CBDs.

3.4. In-Vitro Clustering Design on Scaffold Units

In cellulosomes, cellulases with a dockerin domain have been clustered on a giant scaffold protein with tandemly arranged cohesin and CBD to efficiently degrade

NANO MICRO small

water-insoluble substrates.[10,11] Fierobe et al. produced small chimeric cellulosomes from recombinant cellulolytic enzymes and scaffoldin proteins prepared in *E. coli*. These dockerin-containing enzymes, each of which has a different degradation function, were assembled in vitro on a scaffold protein with two cohesins and CBD to yield a higher activity than that of the same enzymes free in solution.[12,14–16] Recently, some scaffold proteins that are not derived from cellulosomes have been utilized to assemble cellulases. Stable protein 1 (SP1) has a ringlike structure on which 6 homodimers assemble.[36] Heyman et al. fused a cohesin and a dockerin at the terminus of the monomer of SP1 and the catalytic modules of endoglucanase Cel5A, respectively, and 10 catalytic modules were assembled on SP1: the assembled complexes exhibited degradation activity for CMC that was two times greater than that observed for free monomeric Cel5A.[37] The fusion of cohesin in the subunit of rosettasome, which is a thermostable chaperonin with a double-ring structure constructed from 18 subunits, assembled several different cellulases containing a dockerin on a rosettasome to enhance the degradation activity of enzymes to 2–3.5-fold compared with that of a mixture of free enzymes.[38]

Previous studies on the assembly of cellulases on a scaffold protein have focused on the clustering of catalytic modules to enhance the degradation activity of the enzymes. In contrast, in this study, we demonstrated the multivalent effect of CBD on the degradation activity of clustered cellulase complexes: the increase in CBD valence in clustered EglA–CBD complexes markedly enhanced EglA's degradation activity for water-insoluble substrates. Furthermore, we also showed that the utilization of CdSe nanoparticles as scaffold units for assembling catalytic and CBD modules resulted in a significant enhancement of degradation activity relative to that of unclustered enzymes. Although we cannot make a simple comparison between our results and the previously reported results, our results show the potential of CdSe nanoparticles to serve as scaffolds for the design of artificial cellulosomes.

4. Conclusion

In this study, we prepared recombinant catalytic and CBD modules with a biotinylated tag and heterogeneously clustered these modules on streptavidin and on inorganic nanoparticles, thus creating a new design for artificial cellulosomes with multiple CBDs. Heteroclustering of the catalytic and CBD modules resulted in a marked enhancement of the enzyme's degradation activity for amorphous and microcrystalline substrates. The drastic degradation enhancement obtained by clustering the modules on 20 nm CdSe nanoparticles demonstrated the effectiveness of nanoscale scaffold units for increasing CBD valence, which in turn induced the enhancement of degradation activity. The cluster design proposed in this study can easily be used to generate various cellulolytic enzymes with multiple types of CBDs. This design may be utilized as a basic format to devise artificial cellulosomes.

5. Experimental Section

Construction of Expression Vectors for EglA and CBD with a Biotin Acceptor Peptide: The gene coding the EglA from *Aspergillus niger* and second N-terminal CBD of endoglucanase C from *Cellulomonas fimi* was amplified from the vector obtained from Toyota Central R&D Laboratories (Nagakute, Japan) by means of a polymerase chain reaction (PCR) with KOD$^+$ polymerase and two external primers. Each of the gene fragments produced was inserted into the *Nco* I–*Sac* II site of pRA2b vectors containing an IgA hinge linker (SPSTPPTPSPSTPP), biotin acceptor peptide (AviTag; GGLNDIFEAQKIEWH), and poly-histidine tag (HHHHHH) in this order at the C-terminus as reported by Cloutier et al.,[23] and as constructed previously,[8] to produce the plasmids for the EglA and CBD with AviTag at the C-terminus (pRA2b-bioEglA, pRA-bioCBD2endc).

Preparation of EglA and CBD with a Biotinylated Tag: We first transformed *E. coli* BL21 (DE3) with the plasmid of pBIRAcm encoding biotin ligase (Avidity Inc., Aurora, CO) and then transformed the same cells with the plasmids of pRA-bioEglA and pRA-bioCBD2endc, respectively. The transformed *E. coli* cells were incubated in 2 × YT medium containing ampicillin (100 g mL^{-1}) and chloramphenicol (34 g mL^{-1}) at 30 °C. EglA (or CBD) and biotin ligase were induced by adding isopropylthiogalactoside (1 mM) in the presence of 50 μM of D-biotin (Sigma, St. Louis, MO). The harvested cells were centrifuged, and the pellet was suspended in a Tris-HCl solution (50 mM, pH 8.0) with 200 mM NaCl. After sonication, the suspension was centrifuged at 9000 RPM for 30 min, and the supernatant was purified by means of a metal–chelate chromatography column. For EglA, gel filtration chromatography (Hi-Load 16/60 Superdex 75 size exclusion column, GE Healthcare, Little Chalfont, UK) was also performed. The fractionated EglA and CBD with biotinylated tag were collected after the presence of biotin was confirmed in the proteins by means of western-blotting analysis using streptavidin–horseradish peroxidase (GE Healthcare).

Clustering of EglA and CBD with Biotinylated Tag: The biotinylated EglA and CBD were mixed with streptavidin at various concentration (μM) ratios (EglA:CBD:streptavidin = 4:0:0, 4:1.3:0, 4:4:0, 4:12:0, 4:0:1, 4:1.3:1.3, 4:4:2, 4:12:4) in a 50 mM sodium acetate solution (pH 5) with 200 mM NaCl at 4 °C for 24 h. The clustering of added proteins was confirmed by polyacrylamide gel electrophoresis (PAGE) with a blue native-PAGE kit (Invitrogen, Carlsbad, CA): each mixture solutions (18 μL) was mixed with sample buffer (6 μL) and it was loaded onto the native-PAGE gel. For the clustering of EglA and CBD on nanoparticles, CdSe nanoparticles conjugated with streptavidin (particle size: 20 nm, Invitrogen) were mixed with biotinylated EglA and CBD at various concentration (μM) ratios (EglA:CBD:CdSe = 4:0:0.133, 4:1.3:0.178, 4:4:0.267, 4:12:0.533). The binding of streptavidin-conjugated CdSe nanoparticles with EglA and CBD onto PSC substrates was confirmed by mixing with PSC (1 mg mL^{-1}) in a sodium acetate solution (50 mM, pH 5.0, 200 mM NaCl) at 4 °C for 24 h and centrifuging at 6000 RPM for 30 s to detect the fluorescence from CdSe nanoparticles on the PSC substrates.

Size-Exclusion Chromatography: Clustered EglA–CBD complexes on streptavidin were fractionated in a size-exclusion chromatography (SEC) column (Superose 6 10/300 GL, GE Healthcare, Tokyo, Japan) equilibrated with Tris–HCl (50 mM, pH 8.0, 200 mM NaCl). A sample solution (500 μL) was applied to the column at the flow rate of 0.5 mL min^{-1}, and the absorbance of the eluent was monitored at 280 nm.

Enzyme Activity Assays:[39] Clustered EglA–CBD complexes were added to a sodium acetate solution (50 mM, pH 5.0, 200 mM NaCl) containing substrates (1 mg mL^{-1}) at 40°C. All the final concentrations of EglA in the reaction solution were adjusted to 0.4 μM for enzyme activity assays against CMC and PSC, and to 2 μM for the assay against avicel substrates. After incubation intervals (10 min–96 h), the supernatant (5 μL) was mixed with TZ-assay buffer (195 μL of 1 mg mL^{-1} tetrazolium blue chloride, 0.5 M sodium tartrate, 200 mM NaOH, pH 5.0) at 100 °C for 3 min. The reacted solutions were rapidly cooled on ice, and the absorbance of the solutions at 655 nm was measured. The amounts of produced reducing sugars were estimated from the absorbance by normalizing with that of glucose reacted in TZ-assay buffer. For kinetic measurement, clustered EglA–CBD complexes were added in the sodium acetate solution containing PSC (0.5–1 mg mL^{-1}) at the EglA concentrations of 0.4 μM, and the amounts of produced reducing sugars were measured by the TZ-assay at 10–15 s intervals up to 60 s to estimate the reaction rates. Using the reaction rates and substrate concentrations, Lineweaver–Burk plots were applied to calculate k_{cat} and K_m.

Analysis of Binding Affinities of Clustered Complexes to Water-Insoluble Materials: PSC (1.8 mg) was separately added to 50 mM sodium acetate solution (600 μL, pH 5.0, 200 mM NaCl) containing clustered EglA–CBD complexes, and the mixture was incubated for 30 min at 4 °C. After centrifugation, the fluorescence at 331 nm in the supernatant was measured by excitation at 280 nm to quantify the residual proteins in the supernatant.

Acknowledgements

This work was supported by the New Energy and Industrial Technology Development Organization (NEDO) of Japan (M.U.), and by a Scientific Research Grant from the Ministry of Education, Science, Sports, and Culture of Japan (M.U.).

[1] M. A. Rizzo, G. H. Springer, B. Granada, D. W. Piston, *Nature Biotechnol.* **2004**, *22*, 445.
[2] P. Holliger, P. J. Hudson, *Nature Biotechnol.* **2005**, *23*, 1126.
[3] H. L. Greenstone, J. D. Nieland, K. E. de Visser, M. L. H. De Bruijn, R. Kirnbauer, R. B. S. Roden, D. R. Lowy, W. M. Kast, J. T. Schiller, *Proc. Natl. Acad. Sci. USA* **1998**, *95*, 1800.
[4] K. I. Sano, S. Yoshii, I. Yamashita, K. Shiba, *Nano Lett.* **2007**, *7*, 3200.
[5] S. Kang, P. A. Suci, C. C. Broomell, K. Iwahori, M. Kobayashi, I. Yamashita, M. Young, T. Douglas, *Nano Lett.* **2009**, *9*, 2360.
[6] O. I. Wilner, Y. Weizmann, R. Gill, O. Lioubashevski, R. Freeman, I. Willner, *Nature Biotechnol.* **2009**, 4, 249.
[7] R. Leggett, E. E. Lee-Smith, S. M. Jickells, D. A. Russell, *Angew. Chem. Int. Ed.* **2007**, *46*, 4100.
[8] M. Umetsu, T. Hattori, S. Kikuchi, I. Muto, T. Nakanishi, H. Watanabe, I. Kumagai, *J. Mater. Res.* **2008**, *23*, 3241.
[9] M. P. Nikitin, T. A. Zdobnova, S. V. Lukash, O. A. Stremovskiy, S. M. Deyer, *Proc. Natl. Acad. Sci. USA* **2010**, *107*, 5827.
[10] E. A. Bayer, J. P. Belaich, Y. Shoham, R. Lamed, *Annu. Rev. Microbiol.* **2004**, *58*, 521.
[11] H. J. Gilbert, *Mol. Microbiol.* **2007**, *63*, 1568.
[12] H.-P. Fierobe, E. A. Bayer, C. Tardif, M. Czjzek, A. Mechaly, A. Bélaïch, R. Lamed, Y. Shoham, J.-P. Bélaïch, *J. Biol. Chem.* **2002**, *277*, 49621.
[13] I. Fendri, C. Tardif, H.-P. Fierobe, S. Lignon S, O. Valette, S. Pagès, S. Perret, *FEBS J.* **2009**, *276*, 3076.
[14] H.-P. Fierobe, A. Mechaly, C. Tardif, A. Bélaïch, R. Lamed, Y. Shoham, J.-P. Bélaïch, E. A. Bayer, *J. Biol. Chem.* **2001**, *276*, 21257.
[15] H.-P. Fierobe, F. Mingardon, A. Mechaly, A. Bélaïch, M. T. Rincon, S. Pagès, R. Lamed, C. Tardif, J.-P. Bélaïch, E. A. Bayer, *J. Biol. Chem.* **2005**, *280*, 16325.
[16] F. Mingardon, A. Chanal, A. M. López-Contreras, C. Dray, E. A. Bayer, H.-P. Fierobe, *Appl. Environ. Microbiol.* **2007**, *73*, 3822.
[17] P. Béguin, M. Lemaire, *Crit. Rev. Biochem. Mol. Biol.* **1996**, *31*, 201.
[18] W. H. Schwarz, *Appl. Microbiol. Biotechnol.* **2001**, *56*, 634.
[19] R. Kumar, S. Singh, O. V. Singh, *J. Ind. Microbiol. Biotechnol.* **2008**, *35*, 377.
[20] S. Khademi, D. Zhang, S. M. Swanson, A. Wartenberg, K. Witte, E. F. Meyer, *Acta Cryst.* **2002**, *D58*, 660.
[21] J. B. Coutinho, N. R. Gilkes, R. A. J. Warren, D. G. Kilburn, C. A. Haynes, *Mol. Microbiol.* **1992**, *6*, 1243.
[22] E. Brun, P. E. Johnson, A. L. Creagh, P. Tomme, P. Webster, C. A. Haynes, L. P. McIntosh, *Biochemistry* **2000**, *39*, 2445.
[23] S. M. Cloutier, S. Couty, A. Terskikh, L. Marguerat, V. Crivelli, M. Pugnières, J. Mani, H. Leisinger, J. Mach, D. Deperthes, *Mol. Immunol.* **2000**, *37*, 1067.
[24] M. Rheinnecker, C. Hardt, L. L. Ilag, P. Kufer, R. Gruber, A. Hoess, A. Lupas, C. Rottenberger, A. Plückthun, P. Pack, *J. Immunol.* **1996**, *157*, 2989.
[25] G. Carrard, A. Koivula, H. Söderlund, P. Béguin, *Proc. Natl. Acad. Sci. USA* **2000**, *97*, 10342.
[26] M. Linder, T. T. Teeri, *J. Biotechnol.* **1997**, *57*, 15.
[27] P. Tomme, A. L. Creagh, D. G. Kilburn, C. A. Haynes, *Biochemistry* **1996**, *35*, 13885.
[28] H. Watanabe, T. Nakanishi, M. Umetsu, I. Kumagai, *J. Biol. Chem.* **2008**, *283*, 36031.
[29] N. Yokoo, T. Togashi, M. Umetsu, K. Tsumoto, T. Hattori, T. Nakanishi, S. Ohara, S. Takami, T. Naka, H. Abe, I. Kumagai, T. Adschiri, *J. Phys. Chem. B*, **2010**, *114*, 480.
[30] T. Hattori, M. Umetsu, T. Nakanishi, T. Togashi, N. Yokoo, H. Abe, S. Ohara, T. Adschiri, I. Kumagai, *J. Biol. Chem.* **2010**, *285*, 7784.
[31] A. L. Creagh, E. Ong, E. Jervis, D. G. Kilburn, C. A. Haynes, *Proc. Natl. Acad. Sci. USA* **1996**, *93*, 12229.
[32] N. Din, N. R. Gilkes, B. Tekant, R. C. Miller, Jr., R. A. J. Warren, D. G. Kilburn, *Bio/Technol.* **1991**, *9*, 1096.
[33] N. Din, H. Damude, N. R. Gilkes, J. C. Miller, R. A. J. Warren, D. G. Kilburn, *Proc. Natl. Acad. Sci. USA* **1994**, *91*, 11383.
[34] R. Pinto, S. Moreira, M. Mota, M. Gama, *Langmuir* **2004**, *20*, 1409.
[35] D. Ciolacu, J. Kovac, V. Kokol, *Carbohyd. Res.* **2010**, *345*, 621.
[36] O. Dgany, A. Gonzalez, O. Sofer, W. Wang, G. Zolotnitsky, A. Wolf, Y. Shoham, A. Altman, S. G. Wolf, O. Shoseyov, O. Almog, *J. Biol. Chem.* **2004**, *279*, 51516.
[37] A. Heyman, Y. Barak, J. Caspi, D. B. Wilson, A. Altman, E. A. Bayer, O. Shoseyov, *J. Biotechnol.* **2007**, *131*, 433.
[38] S. Mitsuzawa, H. Kagawa, Y. Li, S. L. Chan, C. D. Paavola, J. D. Trent, *J. Biotechnol.* **2009**, *143*, 139.
[39] C. K. Jue, P. N. Lipke, *J. Biochem. Biophys. Methods* **1985**, *11*, 109.

Received: November 24, 2010
Published online: February 2, 2011

Journal of Bioscience and Bioengineering
VOL. 111 No. 2, 140–145, 2011

www.elsevier.com/locate/jbiosc

Material-binding peptide application—ZnO crystal structure control by means of a ZnO-binding peptide

Takanari Togashi,[1] Nozomi Yokoo,[2] Mitsuo Umetsu,[3,4,*] Satoshi Ohara,[5] Takashi Naka,[6] Seiichi Takami,[2] Hiroya Abe,[5] Izumi Kumagai,[3] and Tadafumi Adschiri[1]

Advanced Institute for Materials Research, WPI, Tohoku University, 2-1-1 Katahira, Aoba-ku, Sendai 980-8577, Japan,[1] Institute of Multidisciplinary Research for Advanced Materials, Tohoku University, 2-1-1 Katahira, Aoba-ku, Sendai 980-8577, Japan,[2] Department of Biomolecular Engineering, Graduate School of Engineering, Tohoku University, 6-6-11 Aoba, Aramaki, Aoba-ku, Sendai 980-8579, Japan,[3] Center for Interdisciplinary Research, Tohoku University, 6-3 Aoba, Aramaki, Aoba-ku, Sendai 980-8578, Japan,[4] Joining and Welding Research Institute, Osaka University, 11-1 Mihogaoka, Ibaraki, Osaka, 567-0047 Japan,[5] and Innovative Materials Engineering Laboratory, National Institute for Material Science, 1-2-1 Sengen, Tsukuba, Ibaraki 305-0047, Japan[6]

Received 3 July 2010; accepted 23 September 2010
Available online 13 October 2010

Recently, a zinc oxide (ZnO)-binding peptide (ZnOBP) has been identified and has been used to assist the synthesis of unique crystalline ZnO particles. We analyzed the influence of ZnOBP on the crystal growth of ZnO structures formed from zinc hydroxide. The addition of ZnOBP in the hydrothermal synthesis of ZnO suppressed [0001] crystal growth in the ZnO particles, indicating that the specificity of the material-binding peptide for specific inorganic crystal faces controlled the crystal growth. Furthermore, the dipeptides with a partial sequence of ZnO-binding "hot spot" in ZnOBP were used to synthesize ZnO particles, and we found that the presence of these dipeptides more strictly suppressed (0001) growth in ZnO crystals than did the complete ZnOBP sequence. These results demonstrate the applicability of dipeptides selected from material-binding peptides to control inorganic crystal growth.

[**Key words:** Crystal growth control; Dipeptide; Inorganic material synthesis; Material-binding peptide]

The morphology of inorganic materials synthesized in solution is controlled by crystal face growth, and the growth rate of the crystal faces depends on the crystal structure of these materials. The synthesis of metal, semiconductor, and metal oxide particles with controlled shapes is of fundamental and technological interest, because the synthesis of shape-controlled particles allows for tuning of the particles' shape-dependent physical properties; thus, the particles may be optimized for promising applications in optics, catalysis, biosensing, and data storage (1,2). To this end, organic-solution phase (3–5) and liquid–solid-solution phase synthetic transfer routes (6) have been demonstrated to be versatile pathways toward the development of such shape-controlled metal oxide particles, because these methods allow for control of crystal face growth. In all of these methods, organic surfactants play a key role in determining the growth and stability of inorganic particles.

In biology, combinatorial library approaches have allowed researchers to identify artificial peptides and antibodies with affinity for nonbiological inorganic materials (7–10). These material-binding peptides can be used to directly pattern biomolecules and nanoparticles on inorganic substrates (11–13), and some peptides can be used to synthesize nanometer-to-micrometer-sized inorganic particles in neutral aqueous solution at room temperature (14–17). Such wet-chemical techniques, applied under mild conditions, are attracting growing interest because they are potentially useful for the deposition of inorganic materials in or on heat-labile or pH-sensitive organic compounds. Moreover, some materials synthesized by using material-binding peptides have unique crystalline structures, suggesting that material-binding peptides could be used as an interesting method to synthesize anisotropic inorganic particles (14,15,17). However, because the binding and biomineralization mechanisms of material-binding peptides have not yet been elucidated, these substances cannot yet be utilized to control the morphology of synthesized materials. Rational elucidation of the behavior of material-binding peptides in inorganic synthesis would allow these peptides to be utilized in a broad range of biomimetic approaches toward hybrid material synthesis.

Recently, a zinc oxide (ZnO)-binding peptide (ZnOBP) was identified, and the functionalization of ZnOBP via fusion with a cysteine-containing short peptide resulted in the formation of nanometer-sized ZnO crystallines, which were assembled to unique flower-like structures (17). In this study, we analyzed the influence of ZnOBP on the crystal growth of ZnO structures synthesized from zinc hydroxide ($Zn(OH)_2$) and observed the suppression of crystal growth

Abbreviations: SEM, scanning electron microscopy; XRD, X-ray diffraction; ZnO, zinc oxide; ZnOBP, zinc oxide-binding peptide.

* Corresponding author. Department of Biomolecular Engineering, Graduate School of Engineering, Tohoku University, 6-6-11 Aoba, Aramaki, Aoba-ku, Sendai 980-8579, Japan. Tel./fax: +81 22 795 7276.

E-mail address: mitsuo@kuma.che.tohoku.ac.jp (M. Umetsu).

1389-1723/$ - see front matter © 2010, The Society for Biotechnology, Japan. All rights reserved.
doi:10.1016/j.jbiosc.2010.09.013

in the [0001] direction by the addition of ZnOBP in the hydrothermal synthesis of ZnO. The binding properties of ZnOBP have been physicochemically analyzed previously, and a "hot spot" peptide sequence for ZnO binding has been identified (18). A dipeptide with the same sequence as that of the ZnOBP hot spot was also used to synthesize ZnO particles from $Zn(OH)_2$, and critical suppression of ZnO crystal growth was observed. We describe the potential of dipeptide molecules for controlling the morphology control of synthesized materials.

MATERIALS AND METHODS

An organically synthesized peptide with the ZnOBP sequence (EAHVMHKVAPRP), where the amine and carboxyl groups of the main chain at the N- and C-terminus are inactivated by acetylation and amidation, respectively, was purchased from Peptide Institute, Inc. (Osaka, Japan). The amino acids and the dipeptides also were purchased from Peptide Institute, Inc.

For the ZnOBP-assisted synthesis of ZnO particles, a 0.1 M zinc nitrate solution was mixed with the same volume of 0.2 M potassium hydrate to produce $Zn(OH)_2$. The produced $Zn(OH)_2$ was rinsed several times with distilled water, and the final concentration of $Zn(OH)_2$ was adjusted to 0.1 M. After 1 mg of ZnOBP (690 nmol) were added to 1 ml of the $Zn(OH)_2$ solution, the solution was heated in a closed vessel at 95°C for 24 h to synthesize ZnO. The heated solid material was centrifuged, and the precipitates were rinsed several times with distilled water and then dried in vacuo, yielding ZnO particles. The supernatant was analyzed on a size-exclusion chromatography column (Asahipak GS-220 HQ, Shodex, Tokyo, Japan) equilibrated with H_2O. As an alternative ZnO synthesis, the $Zn(OH)_2$ solution was dried at 95°C in an open vessel for 24 h. For the application of amino acids or dipeptide instead of ZnOBP, we added 690 nmol of them in the $Zn(OH)_2$ solution.

For analyzing the structure of synthesized materials, scanning electron microscopy (SEM) images were obtained on a Philips XL30 ESEM instrument operating at 15 keV. Samples were dried in a vacuum and coated with platinum by means of an ion-coating instrument. X-ray diffraction (XRD) patterns were also recorded with a RINT-2000 spectrometer (Rigaku, Tokyo, Japan) with Cu Kα radiation. Samples were dried in a vacuum before XRD experiments.

RESULTS AND DISCUSSION

To analyze the influence of the material-binding peptide on ZnO synthesis, ZnOBP molecules were added to a $Zn(OH)_2$ solution, and the solution was boiled at 95°C for 24 h to synthesize ZnO particles. Without ZnOBP, needle-type ZnO structures were synthesized (Fig. 1a), whereas addition of ZnOBP resulted in the formation of ZnO needles with flattened edges (Fig. 1b). This structural change induced by the addition of ZnOBP was also observed for ZnO synthesized by means of drying rather than boiling. Changing the dehydration process from boiling to drying caused no structural changes in the ZnO particles synthesized without peptides (data not shown); however, the $Zn(OH)_2$ solution containing ZnOBP formed ZnO particles with peanut-like structures when the drying method was used (Fig. 1c). These structural changes imply that the addition of ZnOBP influenced [0001] crystal growth in the resulting ZnO particles. In the drying method, peptide, ZnO ion, and produced ZnO particles are being concentrated in the process of ZnO synthesis. We consider that the gradual concentration change causes the formation of peanut-like structure.

Fig. 2 shows the XRD pattern of synthesized ZnO materials. The needle-type ZnO structures synthesized without ZnOBP exhibited strong diffraction derived from (100) crystal faces (Fig. 2a), whereas the diffraction was relatively weak in the XRD patterns of ZnO particles synthesized by boiling or by drying with ZnOBP (Fig. 2b and c). These results suggest that the presence of ZnOBP during ZnO synthesis suppressed ZnO crystal growth in the [0001] direction, in agreement with the SEM images shown in Fig. 1. Comparison of the XRD patterns of the ZnO particles synthesized by boiling with those obtained by drying with ZnOBP, in the presence of ZnOBP, revealed that the peanut-like ZnO structures obtained by drying had a weaker (100) diffraction than did the ZnO structures obtained by boiling. This difference in diffraction patterns might indicate that the peanut-like structures had more suppressed [0001] crystal orientation, or that they had more (101) crystal faces, than did the ZnO structure obtained by boiling.

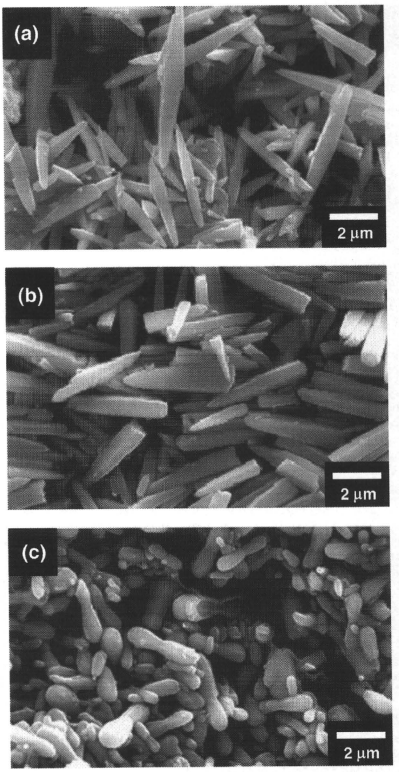

FIG. 1. SEM images of ZnO particles synthesized by boiling 0.1 M $Zn(OH)_2$ solution at 95°C (a) without ZnOBP and (b) with 690 nmol of ZnOBP and of (c) ZnO particles synthesized by drying 0.1 M $Zn(OH)_2$ at 95°C with 690 nmol of ZnOBP.

In our previous report, we identified the sequence around sixth histidine residue in ZnOBP as the hot spot for binding to the ZnO surface (18). Here, we analyzed the influence of the dipeptides with sixth histidine residue, Met-His (fifth–sixth) and His-Lys (sixth–seventh), on ZnO synthesis. When we added the dipeptide Ala-Ala to the ZnO solution as a control peptide and boiled the solution to synthesize ZnO, we observed the same needle-type ZnO particles that were observed for ZnO synthesized without any peptides (Fig. 3a). In contrast, the addition of the dipeptide Met-His resulted in the synthesis of stick-type particles with flatter edges than those of the ZnO rod particles synthesized with intact ZnOBP (Fig. 3b). Moreover, such flattening of synthesized ZnO particle edges was also observed when the dipeptide His-Lys was added to the ZnO solution (Fig. 3c). This flattening of ZnO edges was not observed when mixtures of amino acid monomers (Met and His, His and Lys) were added in the

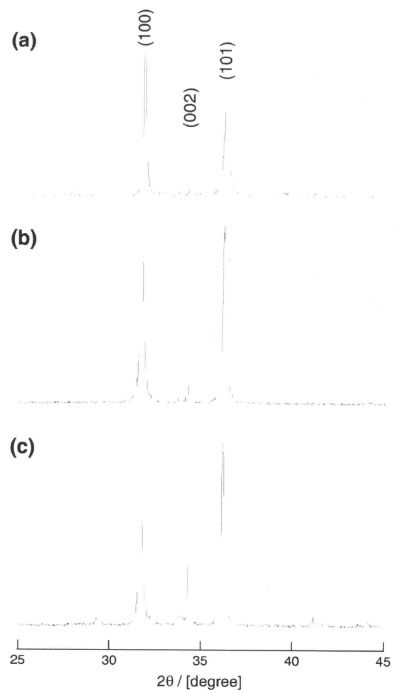

FIG. 2. XRD patterns of ZnO particles synthesized by boiling 0.1 M $Zn(OH)_2$ solution at 95°C (a) without ZnOBP and (b) with 690 nmol of ZnOBP and of (c) ZnO particles synthesized by drying 0.1 M $Zn(OH)_2$ at 95°C with 690 nmol of ZnOBP.

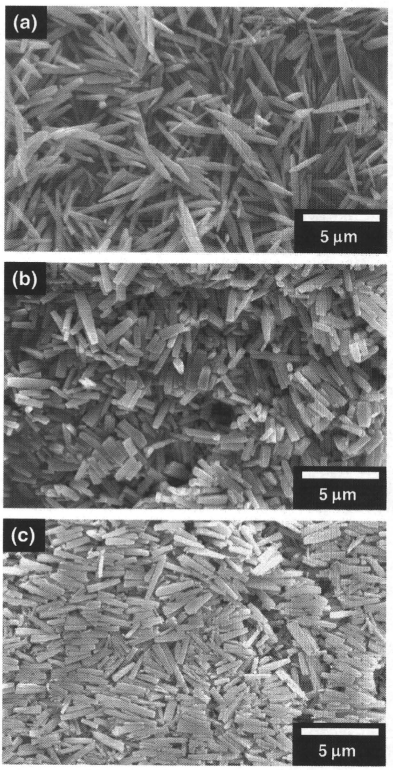

FIG. 3. SEM images of ZnO particles synthesized by boiling 0.1 M $Zn(OH)_2$ solution at 95°C with the dipeptide of (a) Ala-Ala, (b) Met-His, and (c) His-Lys. For all syntheses, the amount of the added dipeptides was 690 nmol.

ZnO synthesis; however, needle-type ZnO particles were formed in those cases (data not shown). In addition, we also analyzed the influence of the dipeptides with third histidine residue, Ala–His (second–third) and His–Val (third–fourth), on ZnO synthesis; however, the presence of the dipeptides did not cause the flattening of ZnO edge (data not shown). Hence, the formation of flattened ZnO edges upon the addition of the Met–His (fifth–sixth) and His–Lys (sixth–seventh) dipeptides indicates that the hot spot sequence in ZnOBP was preferentially bound to the edge area of the ZnO particles in the ZnO synthesis process; it also suggests that the removal of other sequences except for the hot spot residue promotes suppression of [0001] crystal growth in the ZnO synthesis process by capping effect.

To observe the dipeptides' ability to control the structure of synthesized ZnO particles, we synthesized ZnO particles from Zn $(OH)_2$ by boiling the solution with different concentrations of His–Lys dipeptides (Fig. 4). As the amount of added dipeptides increased, the edges of the synthesized ZnO rod particles were flattened at the dipeptide concentration of 690 nmol and the length of the particles decreased. Therefore, the increase in added dipeptides apparently promoted a capping effect for ZnO growth, suppressing the longitudinal growth of ZnO so that the synthesized particles were anisotropically downsized.

ZnO is one of the most widely studied metal oxides for use in solar cells (19), sensors (20), ultraviolet nanolasers (21), and blue-light-emitting diodes (22), because ZnO is a semiconductor with a wide direct band gap that possesses unique optical, acoustic, and electronic properties. This wide variety of applications requires the fabrication of morphologically and functionally distinct ZnO nanostructures; consequently, a large number of studies of morphology control of ZnO have been reported (23–26). In the wet-chemical approaches, kinetic energy barriers, temperature, time, and capping molecules are considered to be factors that can influence the crystal growth of synthesized inorganic materials (27). Among these parameters, capping molecules play two important roles: the creation of appropriate environments where crystal growth is promoted (23) and the selective adsorption of the capping molecules onto specific crystal faces to control the growth rate of capped surfaces (25,28). In

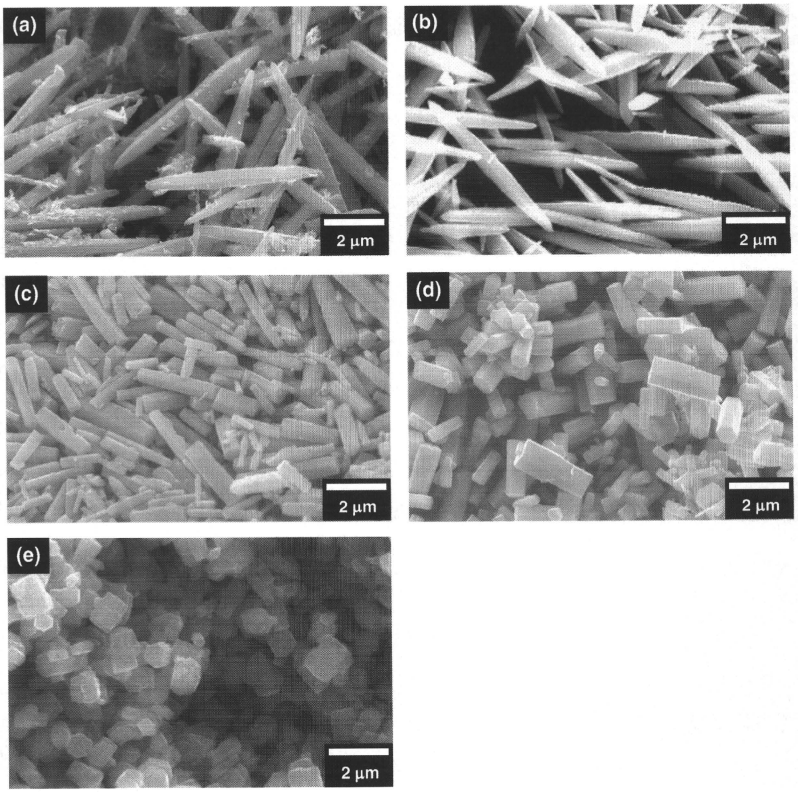

FIG. 4. SEM images of ZnO particles synthesized by boiling $Zn(OH)_2$ solution at 95°C with (a) 0 nmol, (b) 345 nmol, (c) 690 nmol, and (d) 1380 nmol, and (e) 2760 nmol of the dipeptide His-Lys.

this study, we demonstrated the suppression of [0001] crystal growth in ZnO particles in the presence of ZnOBP, particularly in the presence of dipeptides of Met–His and His–Lys, which have been identified as partial sequences of the ZnO-binding hot spot sequence in ZnOBP. Our results suggest preferential adsorption of the hot spot sequence in ZnOBP onto the (0001) crystal faces of ZnO hexagonal structures. For analyzing the stability of ZnOBP at 95 °C in water, we analyzed the peptide solution heated for 24 h, using liquid chromatography (Fig. 5); consequently, few ZnOBPs were hydrolyzed. This result suggests that other peptide sequence in ZnOBP interfere the preferentially binding of Met–His and His–Lys dipeptides onto (0001) crystal faces.

Recently, Tomczak et al. synthesized ZnO from zinc nitrate hexahydrate ($Zn(NO_3)_2$) by using amine molecules at low temperature (29). The addition of another ZnO-binding peptide called Z1 peptide (GLHVMHKVAPPA) inhibited the [0001] crystal growth in the ZnO particles. It should be noted that the sequence HVMHKVAP in the Z1 peptide is identical to the sequence in the hot spot region of ZnOBP. Therefore, the Met–His and His–Lys sequences in HVMHKVAP appear to have a capping effect for ZnO synthesized from both ($Zn(NO_3)_2$) and $Zn(OH)_2$ precursors.

Met, His, and Lys composed of the dipeptide inhibiting the [0001] crystal growth in the ZnO particles (His–Lys and Met–His) have a functional group that can coordinate metal atoms: proteins with metal atoms that are coordinated by these amino acids have been reported (30,31). (1010) and (1120) crystal surfaces of ZnO are formed by the same number of Zn and O, while only one species of atom (Zn or O) appears on (0001) surface (32–34). Although we have no direct evidence, we consider that the dipeptide should prefer the binding onto the Zn-terminated (0001) surface of ZnO. In our study, ZnO morphology could not be controlled by a His amino acid and the dipeptides with His and non-polar amino acids (His–Ala and His–Val:

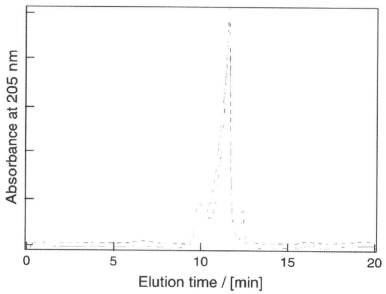

FIG. 5. Size-exclusion chromatography of ZnOBP before boiling at 95 °C for 24 h (solid line) and after boiling at 95 °C for 24 h (dotted line). A 50 μl of 1 mg/ml sample was applied at the flow rate of 0.5 ml/min to a column of Asahipak GS-220 HQ; the absorbance of the eluent was monitored at 205 nm.

second–third and third–fourth sequence of ZnOBP, respectively). These results support our consideration that the presence of two metal-affinitive amino acids in dipeptide results in preference interaction with (0001) crystal face of ZnO.

In our previous report, we synthesized ZnO crystals from $Zn(OH)_2$ at room temperature by using ZnOBP with a GGGSC sequence fused to the binding peptide's C-terminus (17). The addition of GGGSC-fused ZnOBP to $Zn(OH)_2$ required no heat treatment to synthesize ZnO nanoparticles with the size of 10 nm and the synthesized nanoparticles spontaneously assembled to flower-like aggregates. Although the formation mechanism of this flower-like aggregates has not been elucidated yet, the capping effect of ZnOBP at low temperature might have extremely retarded the growth rate of the ZnO crystals, causing the 10-nm nanoparticles to form.

In conclusion, the ZnO-binding peptide ZnOBP, which was composed of the sequence EAHVMHKVAPRP, suppressed [0001] crystal growth in the ZnO particles. Dipeptides containing amino acids found in the identified ZnO-binding hot spot region in ZnOBP promoted the suppression of (0001) growth in ZnO crystals more so than did the complete ZnOBP sequence. Hence, the material-binding peptide's recognition of specific inorganic crystal faces was utilized to control the direction of crystal growth. Peptides with a more specific recognition of crystal faces would afford even greater control of crystal morphology than that demonstrated here. The selection with highly-specific peptides against ZnO crystal face is in progress.

ACKNOWLEDGMENTS

This work was supported by a Scientific Research Grant from the Ministry of Education, Science, Sports, and Culture of Japan (M.U.), by the Industrial Technology Research Grant Program 2005 of the New Energy and Industrial Technology Development Organization (NEDO) of Japan (M.U.), and by Precursory Research for Embryonic Science and Technology from the Japan Science and Technology Agency (JST). This research was also partly supported by the Association for the Progress of New Chemistry foundation (M.U.).

References

1. **Peng, X.:** Mechanisms for the shape-control and shape-evolution of colloidal semiconductor nanocrystals, Adv. Mater., **15**, 459–463 (2003).
2. **Burda, C., Chen, X., Narayanan, R., and El-Sayed, M. A.:** Chemistry and property of nanocrystals of different shapes, Chem. Rev., **105**, 1025–1102 (2005).
3. **Hyeon, T., Lee, S. S., Park, J., Chung, Y., and Na, H. B.:** Synthesis of highly crystalline and monodisperse maghemite nanocrystallites without a size-selection process, J. Am. Chem. Soc., **123**, 12798–12801 (2001).
4. **Rockenberger, J., Scher, E. C., and Alivisatos, A. P.:** A New Nonhydrolytic Single-Precursor Approach to Surfactant-Capped Nanocrystals of Transition Metal Oxides, J. Am. Chem. Soc., **121**, 11595–11596 (1996).
5. **Park, J., An, K., Hwang, Y., Park, J.-G., Noh, H.-J., Kim, J.-Y., Park, J.-H., Hwang, N.-M., and Hyeon, T.:** Ultra-large-scale syntheses of monodisperse nanocrystals, Nat. Mater., **3**, 891–895 (2004).
6. **Wang, X., Zhuang, J., Peng, Q., and Li, Y.:** A general strategy for nanocrystal synthesis, Nature, **437**, 121–124 (2005).
7. **Whaley, S. R., English, D. S., Hu, E. L., Barbara, P. F., and Belcher, A. M.:** Selection of peptides with semiconductor binding specificity for directed nanocrystal assembly, Nature, **405**, 665–668 (2000).
8. **Sarikaya, M., Tamerler, C., Jen, A. K.-Y., Schulten, K., and Baneyx, F.:** Molecular biomimetics: nanotechnology through biology, Nat. Mater., **2**, 577–585 (2003).
9. **Watanabe, H., Nakanishi, T., Umetsu, M., and Kumagai, I.:** Human anti-gold antibodies: biofunctionalization of gold nanoparticles and surfaces with anti-gold antibodies, J. Biol. Chem., **283**, 36031–36038 (2008).
10. **Hattori, T., Umetsu, M., Nakanishi, T., Togashi, T., Yokoo, N., Abe, H., Ohara, S., Adschiri, T., and Kumagai, I.:** High affinity anti-inorganic material antibody generation by integrating graft and evolution technologies. Potential of antibodies as biointerface molecules, J. Biol. Chem., **285**, 7784–7793 (2010).
11. **Park, T. J., Lee, S. Y., Lee, S. J., Park, J. P., Yang, K. S., Lee, K.-B., Ko, S., Park, J. B., Kim, T., Kim, S. K., and other 5 authors:** Protein nanopatterns and biosensors using gold binding polypeptide as a fusion partner, Anal. Chem., **78**, 7197–7205 (2006).
12. **Kacar, T., Ray, J., Gungormus, M., Oren, E. E., Tamerler, C., and Sarikaya, M.:** Quartz binding peptides as molecular linkers towards fabricating multifunctional micropatterned substrates, Adv. Mater., **21**, 295–299 (2009).
13. **Umetsu, M., Hattori, T., Kikuchi, S., Muto, I., Nakanishi, T., Watanabe, H., and Kumagai, I.:** Nanoparticles with affinity for biopolymer: bioassisted room-temperature selective multistacking of inorganic particles on biopolymer film, J. Mater. Res., **23**, 3241–3246 (2008).
14. **Brown, S., Sarikaya, M., and Johnson, E. A.:** Genetic Analysis of Crystal Growth, J. Mol. Biol., **299**, 725–735 (2000).
15. **Naik, R. R., Stringer, S. J., Agarwal, G., Jones, S. E., and Stone, M. O.:** Biomimetic synthesis and patterning of silver nanoparticles, Nat. Mater., **1**, 169–172 (2002).
16. **Mao, C., Flynn, C. E., Hayhurst, A., Sweeney, R., Qi, J., Georgiou, G., Iverson, B., and Belcher, A. M.:** Viral assembly of oriented quantum dot nanowires, Proc. Natl. Acad. Sci. U. S. A., **100**, 6946–6951 (2003).
17. **Umetsu, M., Mizuta, M., Tsumoto, K., Ohara, S., Takami, S., Watanabe, H., Kumagai, I., and Adschiri, T.:** Bioassisted room-temperature immobilization and mineralization of zinc oxide—the structural ordering of zno nanoparticles into a flower-type morphology, Adv. Mater., **17**, 2571–2575 (2005).
18. **Yokoo, N., Togashi, T., Umetsu, M., Tsumoto, K., Hattori, T., Nakanishi, T., Ohara, S., Takami, S., Naka, T., Abe, H., Kumagai, I., and Adschiri, T.:** Direct and selective immobilization of proteins by means of an inorganic material-binding peptide: discussion on functionalization in the elongation to material-binding peptide, J. Phys. Chem. B, **114**, 480–486 (2010).
19. **O'Regan, B., Schwartz, D. T., Zakeeruddin, S. M., and Grätzel, M.:** Electrodeposited nanocomposite n–p heterojunctions for solid-state dye-sensitized photovoltaics, Adv. Mater., **12**, 1263–1267 (2000).
20. **Lin, H.-M., Tzeng, S.-J., Hsiau, P.-J., and Tsai, W.-L.:** Electrode effects on gas sensing properties of nanocrystalline zinc oxide, Nanostruct. Mater., **10**, 465–477 (1998).
21. **Huang, M. H., Mao, S., Feick, H., Yan, H., Wu, Y., Kind, H., Weber, E., Russo, R., and Yang, P.:** Room-temperature ultraviolet nanowire nanolasers, Science, **292**, 1897–1899 (2001).
22. **Tsukazaki, A., Ohtomo, A., Onuma, T., Ohtani, M., Makino, T., Sumiya, M., Ohtani, K., Chichibu, S. F., Fuke, S., Segawa, Y., and other 3 authors:** Repeated temperature modulation epitaxy for p-type doping and light-emitting diode based on ZnO, Nat. Mater., **4**, 42–46 (2005).
23. **Zhang, H., Yang, D., Ji, Y., Ma, X., Xu, J., and Que, D.:** Low temperature synthesis of flowerlike ZnO nanostructures by cetyltrimethylammonium bromide-assisted hydrothermal process, J. Phys. Chem. B, **108**, 3955–3958 (2004).
24. **Pan, Z. W., Dai, Z. R., and Wang, Z. L.:** Nanobelts of semiconducting oxides, Science, **291**, 1947–1949 (2001).
25. **Tain, Z. R., Voigt, J. A., Liu, J., Mckenzie, B., and Mcdermott, M. J.:** Biomimetic arrays of oriented helical Zno nanorods and columns, J. Am. Chem. Soc., **124**, 12954–12955 (2002).
26. **Tain, Z. R., Voigt, J. A., Liu, J., Mckenzie, B., Mcdermott, M. J., Rodriguez, M. A., Konishi, H., and Xu, H.:** Complex and oriented ZnO nanostructures, Nat. Mater., **2**, 821–826 (2003).
27. **Lee, S. M., Cho, S. N., and Cheon, J. W.:** Anisotropic shape control of colloidal inorganic nanocrystals, Adv. Mater., **15**, 441–444 (2003).
28. **Gao, P., Ying, C., Wang, S., Ye, L., Guo, Q., and Xie, Y.:** Low temperature hydrothermal synthesis of ZnO nanodisk arrays utilizing self-assembly of surfactant molecules at solid-liquid interfaces, J. Nanopart. Res., **8**, 131–136 (2006).
29. **Tomczak, M. M., Gupta, M. K., Drummy, L. F., Rozenzhak, S. M., and Naik, R. R.:** Morphological control and assembly of zinc oxide using a biotemplate, Acta Biomater., **5**, 876–882 (2009).

30. **Shibata, N., Inoue, T., Nagano, C., Nishio, N., Kohzuma, T., Onodera, K., Yoshizaki, F., Sugimura, Y., and Kai, Y.:** Novel insight into the copper-ligand geometry in the crystal structure of *Ulva pertusa* plastocyanin at 1.6 Å resolution: structural basis for regulation of the copper site by residue 88. J. Biol. Chem., **274**, 4225–4230 (1999).
31. **Kawakami, N., Toshishige, M., Matsuo, M., Gekko, K., and Michibata, H.:** Characterization of vanadium-binding sites of the vanadium-binding protein Vanabin2 by site-directed mutagenesis, Biochim. Biophys. Acta, **1790**, 1327–1333 (2009).
32. **Özgür, Ü., Alivov, Y. I., Liu, C., Teke, A., Reshchikov, M. A., Doğan, S., Avrutin, V., Cho, S.-J., and Morkoç, H.:** A comprehensive review of ZnO materials and devices, J. Appl. Phys., **98**, 041301-1-109 (2005).
33. **Dulub, O., Boatner, L. A., and Diebold, U.:** STM study of the geometric and electronic structure of ZnO(0001)-Zn, (000–1)-O, (10–10), and (11–20) surfaces, Surf. Sci., **519**, 201–217 (2002).
34. **Noguera, C.:** Polar oxide surfaces, J. Phys. Condens. Matter, **12**, R367–R410 (2000).

the FEBS Journal

MINIREVIEW

Protein–protein interactions and selection: generation of molecule-binding proteins on the basis of tertiary structural information

Mitsuo Umetsu[1,2], Takeshi Nakanishi[3], Ryutaro Asano[1], Takamitsu Hattori[1] and Izumi Kumagai[1]

1 Department of Biomolecular Engineering, Graduate School of Engineering, Tohoku University, Sendai, Japan
2 Center for Interdisciplinary Research, Tohoku University, Sendai, Japan
3 Department of Applied Chemistry and Bioengineering, Graduate School of Engineering, Osaka City University, Japan

Keywords
library design; peptide grafting; protein structure; scaffold protein

Correspondence
M. Umetsu, Department of Biomolecular Engineering, Graduate School of Engineering, Tohoku University, Aoba 6-6-11, Aramaki, Aoba-ku, Sendai 980-8579, Japan
Fax: +81 22 795 7276
Tel: +81 22 795 7276
E-mail: mitsuo@kuma.che.tohoku.ac.jp

(Received 29 October 2009, revised 5 February 2010, accepted 24 February 2010)

doi:10.1111/j.1742-4658.2010.07627.x

Antibodies and their fragments are attractive binding proteins because their high binding strength is generated by several hypervariable loop regions, and because high-quality libraries can be prepared from the vast gene clusters expressed by mammalian lymphocytes. Recent explorations of new genome sequences and protein structures have revealed various small, nonantibody scaffold proteins. Accurate structural descriptions of protein–protein interactions based on X-ray and NMR analyses allow us to generate binding proteins by using grafting and library techniques. Here, we review approaches for generating binding proteins from small scaffold proteins on the basis of tertiary structural information. Identification of binding sites from visualized tertiary structures supports the transfer of function by peptide grafting. The local library approach is advantageous as a go-between technique for grafted foreign peptide sequences and small scaffold proteins. The identification of binding sites also supports the construction of efficient libraries with a low probability of denatured variants, and, in combination with the design for library diversity, opens the way to increasing library density and randomized sequence lengths without decreasing density. Detailed tertiary structural analyses of protein–protein complexes allow accurate description of epitope locations to enable the design of and screening for multispecific, high-affinity proteins recognizing multiple epitopes in target molecules.

Introduction

Antibodies are naturally occurring recognition molecules in the immune system, with high binding affinity and specificity. The strong molecular recognition of antibodies plays important roles in the immune system, and it has been applied in therapeutic fields and the detection of disease-associated marker proteins. Various therapeutic and probe antibodies that target biomolecules in living organisms have been selected from the vast gene cluster for antibodies in mammalian lymphocytes by means of hybridoma and *in vitro* selection technologies [1]. This gene cluster can also supply antibodies with affinity for nonbiological materials [2,3]. The advantage of utilizing antibodies to generate molecules with affinity for a target molecule is the ability to

Abbreviations
^{10}FN3, 10th fibronectin type III domain; CDR, complementarity-determining region; CRAb, chelating recombinant antibody; DARPin, designed ankyrin repeat protein; Fv, fragment of the variable region; NCS, neocarzinostatin; scFv, single-chain fragment of the variable region; TPO, thrombopoietin; VEGF, vascular endothelial growth factor; VHH, variable heavy chain of a heavy-chain camel antibody.